Research Article | Vol. 30, No. 22 / 24 Oct 2022 / Optics Express 39652

Optics EXPRESS

Ultracompact virtual reality system with a Pancharatnam–Berry phase deflector

JUNYU ZOU,[1] ZHENYI LUO,[1] EN ZHAO,[2] YI RAO,[2] AND SHIN-TSON WU[1,*]

[1]College of Optics and Photonics, University of Central Florida, Orlando, FL 32816, USA
[2]Goertek Electronics, 5451 Great America Parkway, Suite 301, Santa Clara, CA 95054, USA
[*]swu@creol.ucf.edu

Abstract: We propose an ultracompact virtual reality (VR) system with three optical components: a lenslet array, a Pancharatnam-Berry phase deflector (PBD), and a deflector array. The lenslet array aims to collect and collimate the input light from the display panel. The PBD steers the deviated beams after the lenslet array toward the optical axis so that the image uniformity and angular resolution can be enhanced, which plays a key role to enable this ultracompact design. Finally, the deflector array deflects the collimated beam from each lenslet to the exit pupil to widen the field of view. Such an ultracompact design is particularly attractive for next-generation glasses-like, lightweight VR headsets.

1. Introduction

After several decades of intensive development, virtual reality (VR) has achieved significant improvement [1]. Currently, some commercial VR products have brought fabulous experience to users and enabled new applications in entertainment [2], engineering [3], education [4], and healthcare [5], just to name a few. However, the form factor of current VR headsets is still too bulky, which limits their long-time wearing. The basic optical system of a VR headset consists of a microdisplay located at the focal plane of an imaging optics [6,7]. In recent years, the thickness and weight of the light engine have been reduced significantly, benefiting from the rapid development of flat panel displays [8,9]. Therefore, the remaining improvement of form factor relies on miniaturing the imaging optics. There is urgent need to develop an ultracompact and lightweight VR headset for comfortable long-time wearing.

Figure 1 depicts the VR systems with different kinds of imaging optics. Figure 1(a) is the conventional optical lens system consisting of a display panel and an optical lens. It has a large form factor and weight, and the optical efficiency is relatively low, because only a small portion of the emitted light from microdisplay can be collected by the lens and observed by the user, although it can achieve a decent imaging quality. To reduce the lens weight, a thin Fresnel lens is adopted in the VR system [7], as Fig. 1(b) shows. However, the Fresnel lens has sharp teeth in the imaging region, which will introduce stray light to the system [10,11] and degrade the imaging quality. Figure 1(c) shows the pancake lens system, which takes the advantage of the folded optical pathlength between two optical surfaces. As a result, it can achieve a higher focal power than the conventional lens, provided that the lens form factor remains at the same level [12,13]. By using the pancake lens, both form factor and weight can be reduced significantly. However, a major trade-off is its dramatically reduced optical efficiency (only 25% as compared to the conventional one) due to the employed half mirror [14,15]. Although the holographic optical elements help to mitigate the optical loss in some designs because of the angular selectivity, the overall efficiency is still only about 30% due to the pancake structure [16]. Moreover, the zero-order light leakage and large angle incidence also produce stray light in the Pancake system, which degrades the imaging quality [11]. Currently, the thickness of a pancake-based VR system is still larger than 20 mm [15,17]. To further reduce the system form factor, here we propose

#473275 https://doi.org/10.1364/OE.473275
Journal © 2022 Received 15 Aug 2022; revised 29 Sep 2022; accepted 29 Sep 2022; published 11 Oct 2022

Optics EXPRESS

to use a lenslet array and a deflector array as the imaging optics, as Fig. 1(d) depicts. In such a system, the lenslet aims to collect and collimate the light from microdisplay and then the deflector array can bend the collimated beam toward the exit pupil. Similar design using a lenslet array and Fresnel lens as imaging optics has also been proposed by Bang, et al [18]. Separating the collimating and bending processes help obtain more degrees of freedom during the design, which in turn benefits the imaging quality and eyebox. Compared to other systems in Fig. 1, our proposed system (Fig. 1(d)) enables a more compact form factor and lighter weight. Moreover, most of the collected light will enter the eye pupil so that the optical efficiency is also higher.

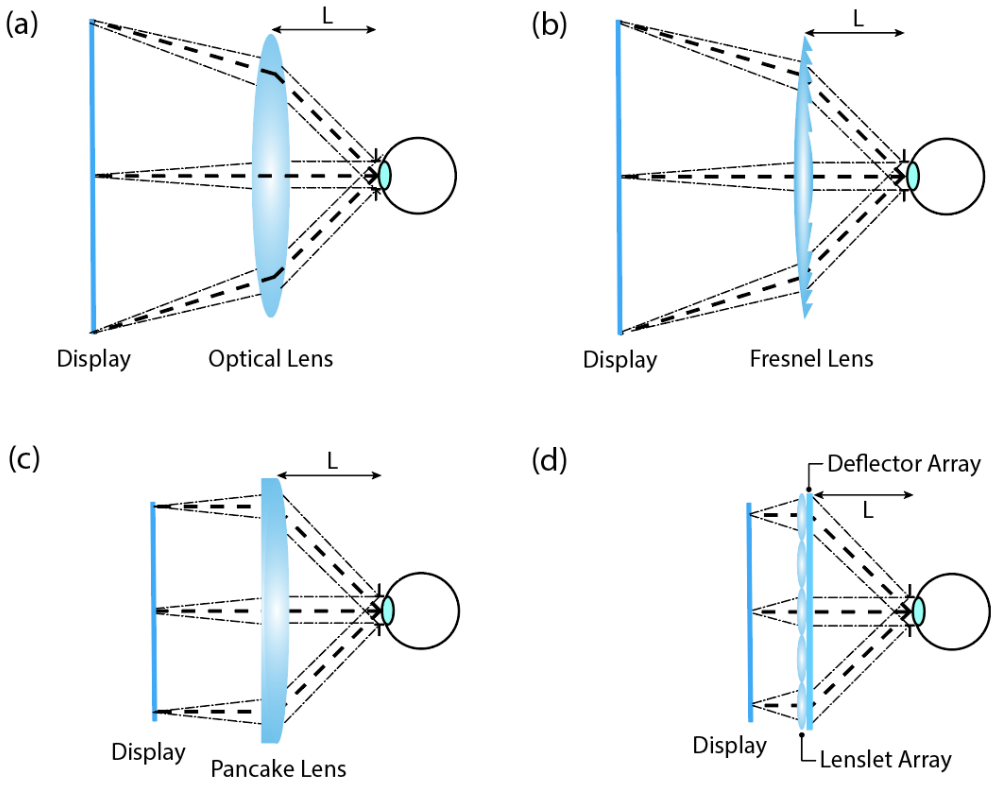

Fig. 1. Schematic of VR systems with different kinds of imaging optics: (a) conventional optical lens, (b) Fresnel lens, (c) Pancake lens, and (d) lenslet array and deflector array. (Eye relief L for different systems are the same)

In our proposed system, the distance between the display panel and the lenslet array will heavily influence the system form factor. Therefore, a short gap between the display panel and the lenslet array is desired. However, the local vignetting such as imaging uniformity could be problematic. If we set the vignetting at 50%, then the distance between the display and the lenslet array (d_1) should be equal to the eye relief (L) for an ideal imaging system, as Fig. 2(a) shows. A comfortable eye relief should be no less than 15 mm. Therefore, the system thickness can be reduced to around 15 mm. Usually, the thickness of the pancake system is larger than 20 mm. If the distance between the display panel and the lenslet array decreases to half an eye relief ($d_2 = L/2$), then the vignetting will increase to 100% (Fig. 2(b)), and the thickness of the system can be less than 10 mm. Under such condition, the nonuniform imaging will be observed, that means some image content will be lost in the view. Therefore, to achieve an ultracompact form factor, we need to narrow down the angular distribution of the collimated beams in Fig. 2(b). Liquid crystal geometric phase optical elements exhibit several attractive features, including

Optics EXPRESS

polarization selectivity, high diffraction efficiency, and compact form factor [19–21], and are promising for near-eye display applications [15,22–24]. These optical elements can be used to weaken the vignetting problem.

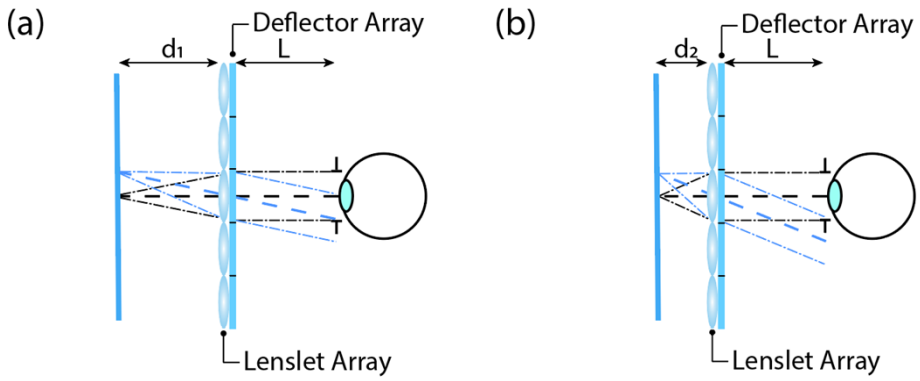

Fig. 2. Schematic of the proposed ultra-compact VR system with different distance between display and imaging optics: (a) the distance equal to eye relief with 50% vignetting, (b) the distance equal to half of the eye relief with 100% vignetting.

In this paper, we propose an ultracompact VR system using a lenslet array to collect and collimate the light emitted from the display panel and a deflector array to bend the collimated beams towards the exit pupil, while keeping an adequate field of view. To further reduce the system form factor, we apply a Pancharatnam-Berry phase deflector (PBD) [19,25] to shorten the distance between the display panel and the imaging optics based on polarization interpolation, which has been experimentally demonstrated. In this work, we focus on the feasibility of applying the PBD to solve the vignetting problem after further reducing the system form factor. The deflector array design and optical image stitching is not discussed.

2. System configuration and operation principles

To prove concept, in experiment we focus on the central lenslet imaging without considering the deflector array. We constructed two VR systems shown in Fig. 3. We used an LCD (Adafruit) as the display panel and two optical lenses with different focal lengths as the central lenslet. The eye relief (L in Fig. 3) of the two systems are the same, which is set to be 20 mm. The focal length of the lenslet in Fig. 3(a) is 20 mm (Thorlabs, AC080-020-A) and in Fig. 3(b) is 10 mm (Thorlabs, AC080-010-A). The aperture of these two lenslets are 8 mm. Therefore, for the same image content from the LCD panel, the image uniformity is expected to be worse for the device configuration in Fig. 3(b). It is worth mentioning that although the system in Fig. 3(b) looks like it has a larger field of view (FOV) than Fig. 3(a), the peripheral pixels have significant vignetting and cannot be observed by users. This means nearly half of the pixels in Fig. 3(b) are "wasted", and the systems in Fig. 3(a)&(b) have the same "effective FOV" (vignetting less than 50%).

A CMOS (Complementary Metal Oxide Semiconductor) camera (TechnoTeam Vision, LMK6 color, with a conoscopic lens) was used to capture the imaging results of these two systems. The input image is shown in Fig. 4(a). Three square dots represent the central and peripheral pixels on the display panel. Figures 4(b) and 4(c) show the imaging results of the VR systems with the 20-mm and 10-mm focal-length lenslet, respectively. In Fig. 4(b), we can clearly see three square dots, but in Fig. 4(c) we can only see the central dot. For the lenlet with a shorter focal length, its collimated beam has a larger off-axis angle. As a result, the peripheral pixels cannot be captured by the camera lens after propagating through the eye relief distance, as Fig. 3(b) depicts. These imaging results indicate that if we shorten the focal length of the lenslet without reconfiguring

Optics EXPRESS

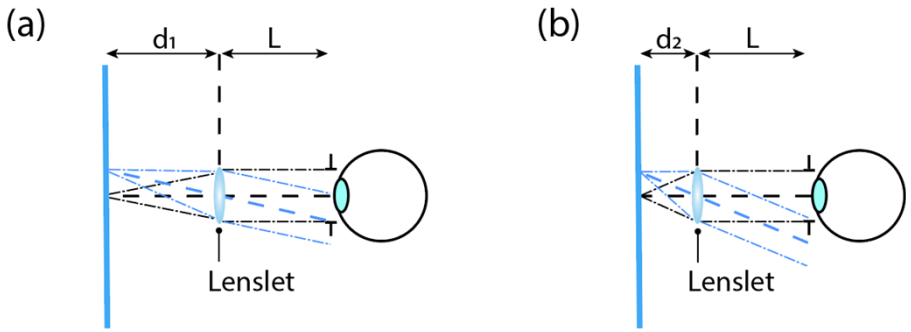

Fig. 3. System configuration with (a) 50% vignetting and (b) 100% vignetting.

the system, some peripheral pixels will be lost, and the imaging uniformity will be problematic. On the other hand, the imaging result in Fig. 4(b) does not show a significant vignetting. The reason is that the aperture size of the conscopic lens is only about 2 mm. To prove it, another camera set (Sony α6100 with 2.8/16 lens) with a larger entrance pupil (around 8 mm) was placed in the same system, and the imaging result is presented in Fig. 4(d). Although this camera cannot capture focused image because its focal length is too long, the intensity difference between the central dot and the peripheral dots is noticeable, as Fig. 4(d) shows.

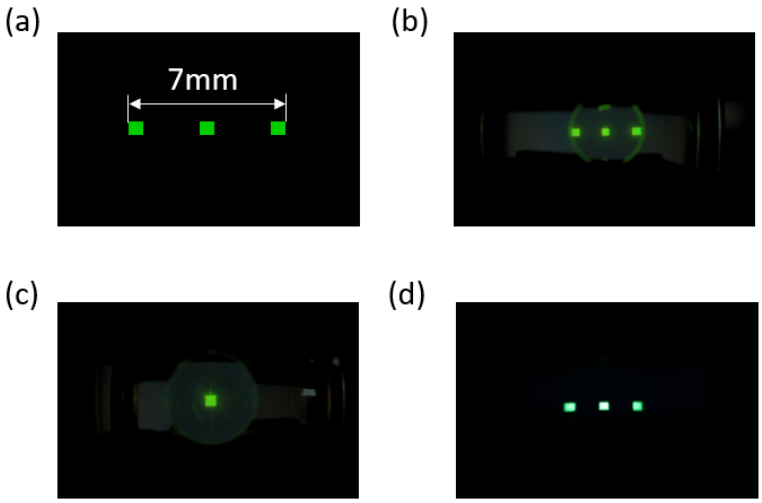

Fig. 4. (a) Image of the input signal. Imaging results of the systems with (b) 50% vignetting and (c) 100% vignetting captured by a 2-mm aperture camera. (d) Imaging result of the 50% vignetting system captured by an 8-mm aperture camera.

To obtain a better vision of the beam intensity distribution, a white screen was placed at the plane of the pupil. The imaging results of the two systems are displayed in Fig. 5. From Fig. 5, we can clearly see three circles, corresponding to the three collimated beams emitted by the three points on the display, respectively. Figure 5(a) represents the result of the system in Fig. 3(a), which has 50% vignetting when the pupil size is 8 mm. After shortening the distance between display and lenslet (Fig. 3(b)), the vignetting increases to near 100% (Fig. 5(b)). It is noticed that the two side-beam intensities are not uniform in Fig. 5(b). The reason is that after shortening the gap between display and lenslet, the off-axis angle is increased for the peripheral points and

Optics EXPRESS

the lenslet has a thickness around 5 mm (for AC080-010-A), so that some part of the off-axis incidence is blocked by the lateral surface of the lenslet.

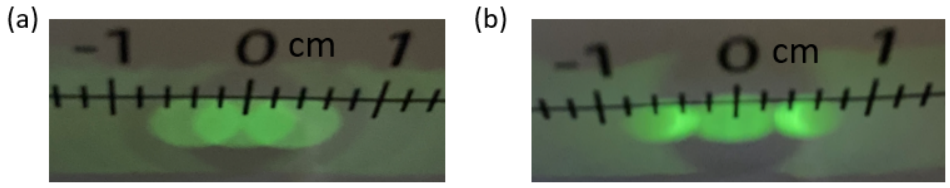

Fig. 5. Beam intensity distribution on the plane of pupil for systems with (a) 50% vignetting and (b) 100% vignetting.

To overcome the increased off-axis angle caused by shortening the distance between display and lenslet, a beam steering process will help mitigate the beam walk-off angle. PB deflector is a polarization dependent device, whose working principle can be explained by following Jones matrix [26]:

$$J'_{\pm} = \frac{1}{\sqrt{2}} \begin{bmatrix} \cos 2\phi & \sin 2\phi \\ \sin 2\phi & -\cos 2\phi \end{bmatrix} \begin{bmatrix} 1 \\ \pm i \end{bmatrix} = \frac{1}{\sqrt{2}} \begin{bmatrix} 1 \\ \mp i \end{bmatrix} e^{\pm 2i\phi}. \tag{1}$$

According to Eq. (1), the output will have an opposite phase change for the left-handed circular polarized (LCP) and the right-handed circular polarized (RCP) inputs. Therefore, if the liquid crystal (LC) directors are patterned with linear change, then this device will work as a PBD, and it will deflect the LCP and RCP inputs to an opposite angle. Based on this property, a PBD can be applied to steer the collimated beams. The working principle is illustrated in Fig. 6. We can divide the pixels on the display panel into LCP and RCP. Let us assume the collimated beam of RCP pixels is deflected to + x direction, while the collimated beam of LCP pixels is deflected to – x direction. Although the diffraction angle of the PBD is angular dependent, the output angles of the collimated beams can be designed to match each other in Fig. 6(a) and (b). In so doing, the vignetting can be reduced by 50%. It is worth mentioning that the RCP and LCP pixels should not be completely symmetric along the lenslet optical axis (Fig. 6(c)), otherwise these two pixels will correspond to two collimated beams with the same direction, which means the resolution will be sacrificed. In theory, the boundary of LCP and RCP pixels should offset the lenslet optical axis as shown in Fig. 6(c), the offset distance should be equal to a quarter pixel pitch. And the imaging content on the display panel should also be modulated because of the interpolation of LCP and RCP pixels. Based on this design, the PBD helps to make better use of the pixels on the display panel and enhance the system angular resolution but keep the system

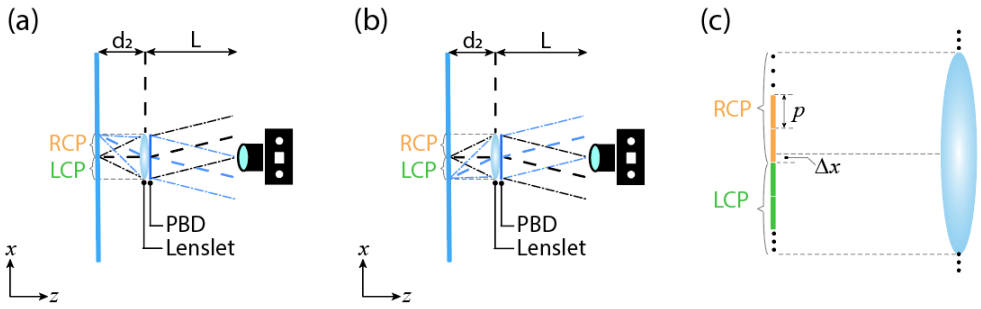

Fig. 6. Schematic of system with (a) RCP pixels and (b) LCP pixels imaging. (c) Example of RCP and LCP pixels off-axis arrangement.

Optics EXPRESS

with the same "effective FOV" (vignetting less than 50%) and form factor compared with the system in Fig. 3(b).

3. Experiment and results

3.1. PBD fabrication

Before fabricating the PBD, the grating period should be calculated. According to Fig. 6(a) and 6(b), the chief ray angle of the edge pixel should be deflected to half, then the grating period of this PBD can be calculated, which is 3.18 μm. Photoalignment method was applied to fabricate this PBD [27,28]. In the beginning, a thin alignment layer (0.2% brilliant yellow dissolved in Dimethyformamide) was spin-coated onto the top surface of a clean glass substrate. Then the substrate was placed in the optical setup shown in Fig. 7 for the holography pattern exposure. After the pattern exposure, two layers of reactive mesogen mixture (RMM) were spin-coated onto the substrate. For each layer, a UV lamp was applied to cure the mixture network right after the spin-coating, so that we can obtain a stabilized polymer film. The RMM includes 96% reactive mesogen RM257 (from LC Matter), 3.9% photo-initiator Irgacure 651 (from BASF), and 0.1% surfactant Zonyl 8857A (from DuPont). This RMM was dissolved in toluene, and the ratio of solute to solvent was 1:5. The fabricated sample was shown in Fig. 8(a), and it was imaging a keyboard. The two ± 1st order diffracted lights can be observed, because the unpolarized ambient light contains both LCP and RCP components. Figure 8(b) is the imaging results of the sample by a polarization microscope (Olympus BX51). The grating structure is clear, and the grating period is 3.11 μm according to the measurement. The thickness of the PBD has been optimized for operating wavelength (532 nm), and the 1st order diffraction efficiency of the PBD can reach 99% at 532 nm after measurement.

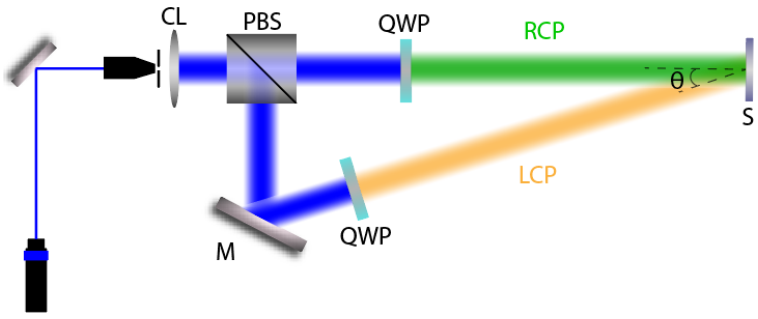

Fig. 7. Experimental setup for fabricating Pancharatnam-Berry phase deflector. CL: collimation lens; PBS: polarized beam splitter; M: mirror; QWP: quarter-wave plate; S: sample.

3.2. System performance

We inserted the fabricated PBD into the system as shown in Fig. 9. The light engine consists of a backlight and a 90° twisted nematic (TN) panel [29]. The output from the TN panel is a linearly polarized light oriented at 45°. We also placed two orthogonal quarter-wave plates (QWP I and QWP II in Fig. 9) side-by-side on the surface of the TN panel, so that the output beam will be converted to LCP and RCP, respectively. The PBD was in close contact with the lenslet back surface and the distance from the TN panel to PBD is around 1 cm. The eye relief is 2 cm. Following the similar process mentioned in Sec. 2 (Fig. 4 and Fig. 5), we applied the input images shown in Fig. 4(a) to the system. The imaging results are presented in Fig. 10. Figure 10(a)

Optics EXPRESS

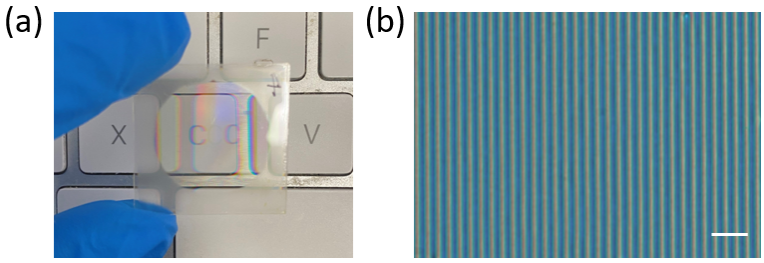

Fig. 8. (a) Photo of the fabricated PBD sample, and (b) polarizing microscope photo of the sample. Scale bar in the picture is 10 μm.

shows the captured photo at the pupil plane. Because the employed light engine in the system has a broad spectrum, the output contains some red component even if the input signal is green. To narrow down the spectral bandwidth, a green color filter whose central wavelength is 532 nm was placed between the PBD and camera. According to the result, the images of the peripheral dots can also be captured by the camera, after the collimated beams are deflected by the PBD. The central square dot is split into two parts and merged into the two peripheries, respectively. The beam intensity distribution is shown in Fig. 10(b). The collimated beam of the central square dot is also split into two parts with equal intensity and merged to the two peripheral dots.

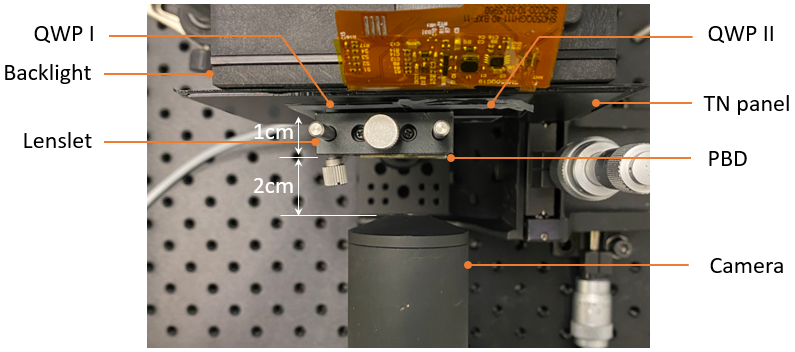

Fig. 9. Photo (top view) of the optical system setup.

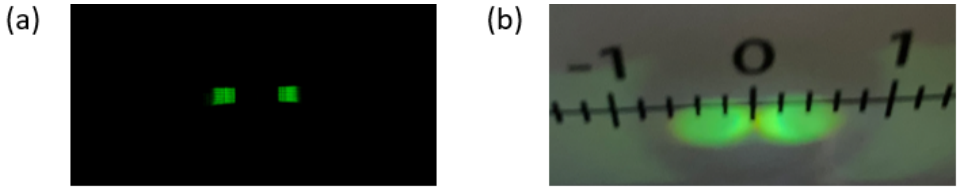

Fig. 10. (a) Imaging result and (b) intensity distribution at pupil plane of the ultra-compact VR system with a PBD.

The operation principle of applying a PBD to shorten the distance between the light engine and the lenslet has been illustrated in Fig. 3 and Fig. 6 with confirming experimental results shown in Fig. 4 and Fig. 10. To demonstrate feasibility of the proposed system for a VR display, we use green color ABCD letters (Fig. 11(a)) as the input, and the imaging results are shown in Fig. 11(b). In our design, the pixels on the left half and right half emit LCP and RCP light,

Optics EXPRESS

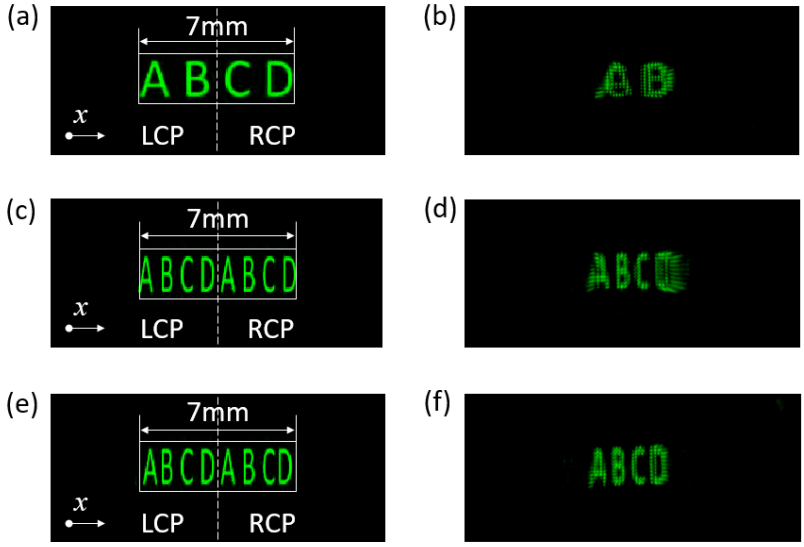

Fig. 11. (a), (c), (e) Input image contents during the rendering and (b), (d), (f) the corresponding imaging results.

respectively. That means, in Fig. 11(a) and 11(b), letters A and B are LCP and letters C and D are RCP. Then the collimated beams corresponding to A and B will be deflected towards $-x$ direction and the collimated beams corresponding to C and D will be deflected towards $+x$ direction. Therefore, in the imaging result shown in Fig. 11(b), the letters A and B are overlapped with C and D, respectively. Next, we rendered the input signal to make the output as the desired imaging content, ABCD. Based on the system principle, we divided the pixels in Fig. 11(a) (pixels in the white box) into odd and even columns. The odd column pixels are joined together to form the left half of the signal in Fig. 11(c), and the even column pixels form the right half. The rendered picture is shown in Fig. 11(c). Each character is split into two parts with LCP and RCP pixels. The imaging optics will interpolate these two parts together and the result is depicted in Fig. 11(d). According to the results, letters B and C are well reproduced, but A and D are not. This is because the LCP A on the left and RCP D on the right are not deflected with a large enough angle after PBD, so that they are not well interpolated to the RCP A and LCP D, respectively. This problem originates from the angular response of PBD and lenslet aberration, which will be discussed in details in later section. On the other hand, the LCP A and RCP D on the two sides hit the edge of the lenslet so that the aberration is significant. To improve the rendering result, we shorten the distance between the LCP A and B, and the distance between the RCP D and C, which is shown in Fig. 11(e). In this way, it can correct the deflection angle of the LCP A and RCP D and reduce the aberration. The improved result is depicted in Fig. 11(f). All the characters are well reproduced and the feasibility of the proposed ultracompact VR system with a PBD is demonstrated. In the experimental results, the rasterized pattern can be observed. This is because the resolution of the display panel (5.0" 800*400 from Adafruit) is low. If the system applied a high resolution display panel, this pattern can be eliminated.

4. Discussion

During the rendering process, we notice that the deflection angles of the characters are slightly different, which will cause some characters not interpolating well, just like the condition shown in Fig. 11(d). This is because the deflection angle of PBD is dependent on the incident angle. We measured and calculated the deflection angles of the applied PBD with different input angles,

Optics EXPRESS

and results are shown in Fig. 12(a). At normal incidence, the deflection angle is around 9.8°; but as the input angle increases to 20°, the deflection angle shifts to 10.9°. It is easy to see that the deflection angle increasing with the incident angle, which means the characters on the margin will be over-deflected. However, according to the result in Fig. 11(d), the LCP A and RCP D are under-deflected. To find out the reason, the lenslet imaging profile is plotted by Zemax as Fig. 12(b) shows. The marginal ray of the boundary pixels, whose off-axis distance is 3.5 mm, will be bent with a larger angle than the chief ray, because of the lenslet aberration. In Fig. 12(b), the output angle of the chief ray is 19°, but the marginal ray output angle is as large as 25°, and for the boundary pixels, the marginal rays dominate the energy going through the eye pupil. It explains why the PBD under-deflects the margin characters even if they have larger deflection angles.

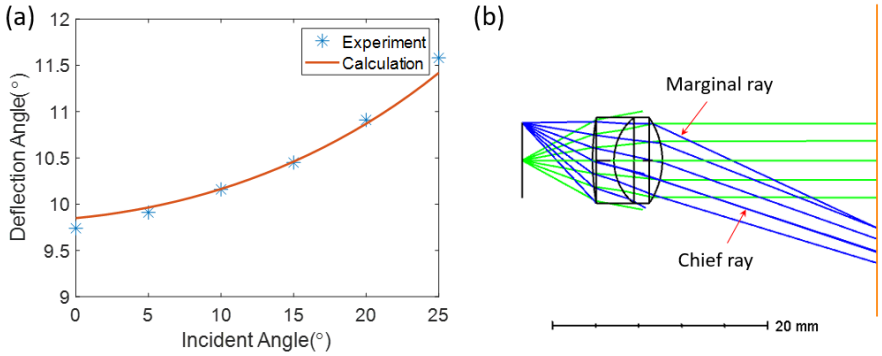

Fig. 12. (a) Angular response of the fabricated PBD and (b) imaging profile of the lenslet in Zemax.

In experiment, we notice that the boundary pixels suffer from significant aberration. Even if we can customize the lenslet array performance to minimize the aberration in the future, this problem cannot be eliminated completely. Therefore, the boundary pixels will be sacrificed. One solution is to segment the display panel to different sub-panels corresponding to each lenslet, as Fig. 13 shows. In this way, the resolution of the sub-panels might be varied, so that a foveated display system can be designed. As indicated in Fig. 13, the central sub-panel covers the foveated region and requires a high-resolution panel. Medium resolution sub-panels surround the central sub-panel and perform as the transition area from high resolution to low resolution. The peripheral region is covered by low resolution sub-panels.

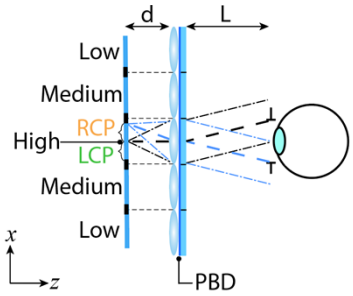

Fig. 13. Schematic of the foveated ultra-compact VR system.

For full color performance, the PBD can be fabricated with dual-twist or multi-twist structure [26,30,31] to achieve high diffraction efficiency at primary RGB wavelengths. However, the

Optics EXPRESS

diffraction angles for different color input will not be the same. Therefore, when the input signal contains multiple colors, the signal of each color should be rendered individually.

On the other hand, the imaging content in Fig. 11 mainly expands in X direction. If the image further extends along Y direction, then the vignetting will also appear. This approach can be extended to two dimensions. In Y direction, the same process can be applied, but it requires active wave plates to modulate the polarization states of the pixels, and the system needs time-multiplexing, which is shown in Fig. 14(a). Another method is to reduce the pixels in Y direction, as depicted in Fig. 14(b), because the human eye has a smaller FOV in the vertical direction than that in the horizontal direction.

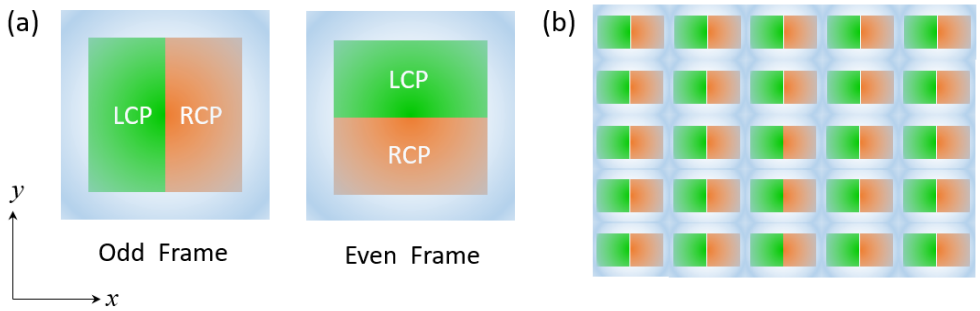

Fig. 14. Two methods for two-dimensional operation: (a) active waveplate with time multiplexing; (b) reducing the number of pixels in Y direction.

In this paper, the feasibility of applying PBD to solve the vignetting problem in the ultra-compact VR system has been proven. In the proposed system, there is a third optical component, the deflector array, which deflects rays that pass through the lenslet array and PBD towards the eye pupil. The design of the deflector array and optical image stitching is another interesting research topic, which will be our future work.

5. Conclusion

We proposed an ultracompact VR system, whose imaging optics consisting of a lenslet array, a deflector array, and a PBD. The lenslet array aims to collect the light emitted from the display panel while the deflector array functions to bend the beams toward the eyebox. We have experimentally demonstrated that the PBD plays a key role in the polarization interpolation, which helps to reduce the system vignetting. The fabricated PBD is a thin polymer film and can be directly laminated to the lenslet without increasing the system's form factor and weight noticeably. The system has a total thickness around 1 cm with 8mm eyebox (50% vignetting) and 20mm eye relief. Image rendering and angular calibration process are also proven. The proposed ultracompact VR structure can significantly reduce the system form factor, and its widespread applications for VR systems are foreseeable.

Funding. Goertek Electronics.

Acknowledgments. The authors are indebted to Jason Adams and TechnoTeam Vision for providing the CMOS camera, which play a crucial role in our experiment. The authors are also indebted to Guanjun Tan for the stimulating discussion.

Disclosures. The authors declare no conflicts of interest.

Data availability. Data underlying the results presented in this paper are not publicly available at this time but may be obtained from the authors upon reasonable request.

References

1. M. L. Heilig, "Sensorama simulator," U.S. patent 3,050,870 (August 28, 1962).

Optics EXPRESS

2. M. Zyda, "From visual simulation to virtual reality to games," Computer **38**(9), 25–32 (2005).
3. L.P. Berg and J.M. Vance, "Industry use of virtual reality in product design and manufacturing: a survey," Virtual Reality **21**(1), 1–17 (2017).
4. H. Ardiny and E. Khanmirza, "The Role of AR and VR Technologies in Education Developments: Opportunities and Challenges," in *6th RSI International Conference on Robotics and Mechatronics (IcRoM)* (2018), pp. 482–487.
5. J. Pottle, "Virtual reality and the transformation of medical education," Future Healthc J. **6**(3), 181–185 (2019).
6. K. Yin, EL. Hsiang, J. Zou, Y. Li, Z. Yang, Q. Yang, PC. Lai, C. L. Lin, and S. T. Wu, "Advanced liquid crystal devices for augmented reality and virtual reality displays: principles and applications," Light: Sci. Appl. **11**(1), 161 (2022).
7. B. C. Kress, *Optical Architectures for Augmented-, Virtual-, and Mixed-reality Headsets*, (SPIE press, 2020).
8. H. Chen, J. H. Lee, B. Y. Lin, S. Chen, and S. T. Wu, "Liquid crystal display and organic light-emitting diode display: present status and future perspectives," Light: Sci. Appl. **7**(3), 17168 (2018).
9. J. Xiong, E.L. Hsiang, Z. He, T. Zhan, and S. T. Wu, "Augmented reality and virtual reality displays: emerging technologies and future perspectives," Light: Sci. Appl. **10**(1), 216 (2021).
10. D. J. Lamb and L. W. Hillman, "Computer modeling and analysis of veiling glare and stray light in Fresnel lens optical system," Proc. SPIE **3779**, 344–352 (1999).
11. Y. Geng, J. Gollier, B. Wheelwright, F. Peng, Y. Sulai, B. Lewis, N. Chan, W.S.T. Lam, A. Fix, D. Lanman, and Y. Fu, "Viewing optics for immersive near-eye displays: pupil swim/size and weight/stray light," Proc. SPIE **10676**, 19–35 (2018).
12. J. A. LaRussa and A. T. Gill, "The Holographic Pancake Window^{TM}," Proc. SPIE **0162**, 120–129 (1978).
13. T. L. Wong, Z. Yun, G. Ambur, and J. Etter, "Folded optics with birefringent reflective polarizers," Proc. SPIE **10335**, 103350E (2017).
14. A. Maimone and J. Wang, "Holographic optics for thin and lightweight virtual reality," ACM Trans. Graph. **39**(4), 67–70 (2020).
15. J. Zou, T. Zhan, E.L. Hsiang, X. Du, X. Yu, K. Li, and S.T. Wu, "Doubling the optical efficiency of VR systems with a directional backlight and a diffractive deflection film," Opt. Express **29**(13), 20673–20686 (2021).
16. O. Cakmakci, Y. Qin, P. Bosel, and G. Wetzstein, "Holographic pancake optics for thin and lightweight optical see-through augmented reality," Opt. Express **29**(22), 35206–35215 (2021).
17. B. A. Narasimhan, "Ultra-Compact pancake optics based on ThinEyes super-resolution technology for virtual reality headsets," Proc. SPIE **10676**, 359–366 (2018).
18. K. Bang, Y. Jo, M. Chae, and B. Lee, "Lenslet VR: thin, flat and wide-FOV virtual reality display using fresnel lens and lenslet array," IEEE Trans. Visual. Comput. Graphics **27**(5), 2545–2554 (2021).
19. M. J. Escuti, C. Oh, C. Sánchez, C. Bastiaansen, and D. J. Broer, "Simplified spectropolarimetry using reactive mesogen polarization gratings," Proc. SPIE **6302**, 21–31 (2006).
20. N. V. Tabiryan, S. V. Serak, D. E. Roberts, D. M. Steeves, and B. R. Kimball, "Thin waveplate lenses of switchable focal length - new generation in optics," Opt. Express **23**(20), 25783–25794 (2015).
21. K. Gao, C. McGinty, H. Payson, S. Berry, J. Vornehm, V. Finnemeyer, B. Roberts, and P. Bos, "High-efficiency large-angle Pancharatnam phase deflector based on dual-twist design," Opt. Express **25**(6), 6283–6293 (2017).
22. T. Zhan, J. Zou, J. Xiong, X. Liu, H. Chen, J. Yang, S. Liu, Y. Dong, and S. T. Wu, "Practical chromatic aberration correction in virtual reality displays enabled by large-size ultra-broadband liquid crystal polymer lenses," Adv. Opt. Mater. **8**(2), 1901360 (2020).
23. J. Zou, L. Li, and S.T. Wu, "Gaze-matched pupil steering Maxwellian-view augmented reality display with large angle diffractive liquid crystal lenses," Adv. Photonics Res. **3**(5), 2100362 (2022).
24. S. Moon, C.K. Lee, S.W. Nam, C. Jang, G.Y. Lee, W. Seo, G. Sung, H.S. Lee, and B. Lee, "Augmented reality near-eye display using Pancharatnam-Berry phase lenses," Sci. Rep. **9**(1), 6616 (2019).
25. S. Pancharatnam, "Achromatic combinations of birefringent plates. Part II. An achromatic quarter wave plate," Proc. – Indian Acad. Sci., Sect. A **41**(4), 137–144 (1955).
26. J. Zou, T. Zhan, J. Xiong, and S. T. Wu, "Broadband wide-view Pancharatnam–Berry phase deflector," Opt. Express **28**(4), 4921–4927 (2020).
27. V. G. Chigrinov, V. M. Kozenkov, and H. S. Kwok, *Photoalignment of Liquid Crystalline Materials: Physics and Applications* (Wiley, 2008).
28. K. Ichimura, "Photoalignment of liquid-crystal systems," Chem. Rev. **100**(5), 1847–1874 (2000).
29. M. Schadt and W. Helfrich, "Voltage-dependent optical activity of a twisted nematic liquid crystal," Appl. Phys. Lett. **18**(4), 127–128 (1971).
30. C. Oh and M. J. Escuti, "Achromatic diffraction from polarization gratings with high efficiency," Opt. Lett. **33**(20), 2287–2289 (2008).
31. R. K. Komanduri, K. F. Lawler, and M. J. Escuti, "Multi-twist retarders: broadband retardation control using self-aligning reactive liquid crystal layers," Opt. Express **21**(1), 404–420 (2013).